



Usage of Tyre Derived Aggregates as backfill around buried pipelines crossing strike-slip faults; model tests

Mustafa Karaman¹ · Hasan Emre Demirci² · Nurhan Ecemis¹ ·
Subhamoy Bhattacharya³ 

Received: 23 May 2021 / Accepted: 8 March 2022 / Published online: 9 April 2022
© The Author(s) 2022

Abstract

Buried pipelines crossing active faults are exposed to excessive soil forces under fault movements due to large relative movement between pipes and the soil surrounding them. As a result, extreme longitudinal strains develop within pipelines under large fault movements and this leads to pipeline failures. Several seismic mitigation techniques were proposed to improve the performance of buried pipelines crossing active faults. In this study, the potential of using Tyre Derived Aggregates (TDA) as a backfill material for mitigating the effects of strike-slip faulting are investigated through physical model tests. First, the details of the physical model test setup and model configuration are presented. Then a comparative study is carried out to study the effect of TDA content in the backfill and trench configurations on TDA mitigation. Model tests revealed that using a sloped trench with 100% TDA content in the backfill can decrease peak axial pipe strains up to 62% and peak bending strains up to 19%. It is observed that enlarging the trench and using an inclined trench improve the performance of the TDA mitigation technique.

Keywords Physical model tests · Backfill-Tyre Derived Aggregates (TDA) · Seismic mitigation technique · Fault crossings · Buried continuous pipelines

1 Introduction

Pipelines are reliable means of transporting water, gas, oil, sewage, and other liquids. Due to these missions, a nation's services, industries, and economy highly depend on them. Therefore, it is very essential that they always remain operational. Pipelines are sometimes laid above the ground in geo-hazardous areas, for example, the Alaskan Pipeline whereas

✉ Subhamoy Bhattacharya
S.Bhattacharya@surrey.ac.uk

¹ Izmir Institute of Technology, Izmir, Turkey

² Izmir Katip Celebi University, Izmir, Turkey

³ University of Surrey, Guildford, UK

they are often buried below the ground in areas where ground conditions are suitable, by taking into account city planning, safety, environmental and economic factors. They cross seismic areas and are under threat due to permanent ground deformations (PGDs) caused by earthquakes. Observations from past earthquakes highlighted that buried pipelines are highly vulnerable to earthquake-induced PGDs. PGDs are events induced by earthquakes such as faults, landslides, ground settlement due to liquefaction, liquefaction-induced lateral spreading. PGDs imposed large stresses on buried pipelines and pipeline damage such as tensile failure, beam buckling, local buckling, and joint failure occurred because of the excessive longitudinal stresses.

Several researchers proposed seismic mitigation methods to improve the performance of buried pipelines crossing PGD zones. As shown in Fig. 1, seismic mitigation techniques for pipelines crossing PGD areas are basically grouped as soil-pipe friction reduction and pipe strengthening. Soil-pipe friction reduction techniques target to minimize axial pipe strains that develop due to friction forces at the soil-pipe interface. On the other hand, pipe strengthening techniques are used to provide additional stiffness to pipelines to reduce both bending and axial strains. The techniques of soil-pipe friction reduction include placing pipelines within concrete culverts without using backfill soil (Melissianos et al. 2017), using geof foam instead of using soil backfill over pipelines (Choo et al. 2007), using pumice as backfill for the trench (Melissianos et al. 2017), wrapping pipelines with friction-reducing geotextiles (Gantes and Bouckovalas 2013; Trifonov and Cherniy 2016), using geogrids and geo-cells between pipelines (Gantes and Melissianos 2016) and the surrounding soil and trench enlargement (Kouretzis et al. 2013; Gantes and Melissianos 2016). Pipe strengthening techniques include increasing the wall thickness of pipelines (Vazouras et al. 2010; Karamanos et al., 2014), wrapping pipelines with composite wraps (Mokhtari and Alavi Nia 2015; Trifonov and Cherniy 2016), and upgrading the steel grade (Vazouras et al. 2010; Gantes and Bouckovalas 2013). There are other mitigation techniques that are placing pipelines above the ground (Honegger and Nyman 2004), linking flexible joints between adjacent pipe parts at fault crossing zones (Melissianos et al. 2016), creating a pre-defined buckling pattern (Hasegawa et al. 2014), and using a protective device (Zhang et al. 2016).

Placing pipelines above the ground on the supports eliminates soil-pipe interaction under PGDs so that pipelines are not subjected to soil movements during faulting. As flexible joints can absorb rotations at the joints, pipe segments remain undeformed and unstressed. Localized buckling pattern allows controlling the location and mode of pipe

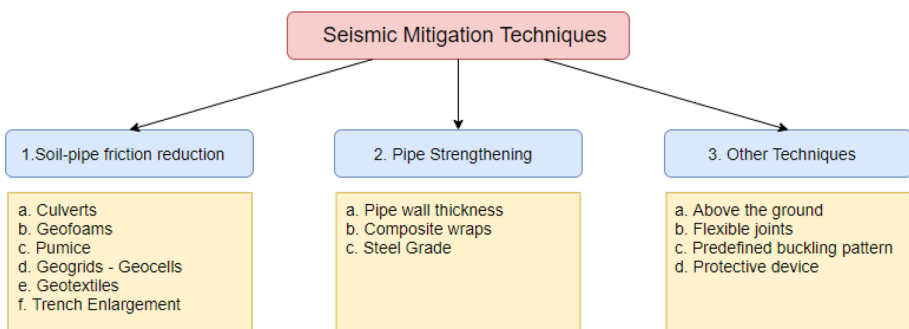


Fig. 1 Seismic mitigation techniques for pipelines crossing PGD zones

failure and increases the performance of pipelines crossing PGDs. Protective devices apply external hydrostatic pressure on pipelines, and this helps to avoid the occurrence of local buckling at pipe walls.

Besides seismic mitigation techniques mentioned above, recently, Tyre Derived Aggregates (TDA) as a backfill material were also used to improve the performance of buried pipelines crossing PGD zones. TDAs, are compressible and flexible materials compared to stiffer traditional sand backfill. Also, TDA is a relatively lightweight material that reduces the earth pressure imposed on buried structures. Also, The European Tyre and Rubber Manufacturers' Association (ETRMA 2019) published data that cover 32 countries and mentioned that 3.5 megatons of scrap tyres were generated in 2018. As a summary of the report, 53.6% of total scrap tyres were used as granulated in several industries. Not only the physical and engineering properties of TDA is quite favourable, but also TDA manufacturing is the largest part of the rapidly growing scrap tyre recycling industry. Therefore, TDA has been used in several geotechnical applications such as lightweight backfills, highway embankments, backfill material for retaining structures, and soil reinforcement.

Sim et al. (2012) performed a series of shake table tests to model buried pipelines crossing a vertical fault. The model pipelines used in their study were buried in dry Toyoura sand as well as a TDA backfill trench surrounded by Toyoura sand. The test setup was capable of simultaneously applying seismic shaking and faulting. The test results showed that using TDA as a backfill material surrounding the pipe reduced the bending moments that developed due to simultaneous seismic shaking and faulting.

Ni et al. (2018a, b, c) conducted a finite element simulation to investigate the behaviour of rigid pipes buried in TDA backfill. They concluded that TDA reduces the loads on rigid pipes like other compressible materials such as geogrid and sawdust. They also performed a parametric study to optimize the design considering relative stiffness between soil and TDA, the spacing between the TDA zone and the pipe, and the geometry of the TDA zone. They found that the earth pressure at the pipe crown and invert was significantly reduced. However, lateral pressure at the spring-line of the pipe was slightly decreased. The increase of the width of the TDA zone reduced earth pressures around the pipe but the change in the thickness of the TDA zone did not influence the earth pressures on the pipe. A larger relative stiffness between the soil and the TDA resulted in a reduction of earth pressures on pipes since more significant positive arching effect occurs with increasing relative soil-TDA stiffness.

Ni et al. (2018a, b, c) performed a numerical study to investigate the seismic mitigation potential of using TDA as a backfill material for buried pipelines crossing strike-slip faults. They showed that using a TDA backfill trench is more effective than other conventional mitigation techniques including burying the pipe at a shallower depth, increasing the pipe wall thickness, upgrading the pipe material grade, and replacing native soils. The optimum fault crossing angle for TDA mitigation technique to minimize pipe strains was found to be equal to 90° . It was seen that enlarging the TDA trench reduced pipe strains under fault movements as enlarging the TDA trench reduced the interaction between buried pipes and surrounding native soil outside the trench.

Both studies validated their numerical model by comparing the numerical results to the 1 g shaking table tests of Sim et al. (2012).

The related literature points out that, very limited studies particularly experimental works were carried out to study the potential use of TDA as backfill material for buried pipelines crossing PGD zones. Hence, there is a high need to investigate the performance of this seismic mitigation technique (backfilling the pipe with TDA) for buried continuous pipelines crossing strike-slip faults.

In this study, first, a physical model test setup that was used to understand the performance of the Tyre Derived Aggregates as a seismic mitigation technique for buried continuous pipelines crossing strike-slip faults were introduced. Then several physical model tests were carried out to assess the performance of Tyre Derived Aggregates (TDA) as a backfill material of buried pipeline at fault crossings with five different trenches of TDA. The results from the model tests clarified the effects of (1) percentage of TDA in trench backfill, (2) trench shape, and (3) trench dimensions on the behaviour of buried pipelines crossing strike-slip faults. A better understanding of effects of backfill materials to pipeline behaviour crossing strike-slip fault will enable a more appropriate pipeline design for the engineers in practice.

2 Experimental study

2.1 Material

In the experimental study, Red Hill 110 sand and TDA with a mean particle size of 3 mm were used. Figure 2a shows particle size distribution of Red Hill 110 dry sand and TDA. The median particle diameter of the Red Hill sand (D_{50}) is 0.144 mm. The dry unit weight of the sand (γ_{sand}) is 13 kN/m³ at the relative density (D_r) of 35%. The median particle diameter (D_{50}) of the TDA is obtained as 3 mm. The unit weight of the TDA (γ_{TDA}) is 4.73 kN/m³. Figure 2b shows the photo of the TDA particles used in the experiments.

Specific gravity, minimum and maximum void ratio of Red Hill 110 dry sand were obtained by element tests (ASTM D4254-00, 2000; ASTM D4253-00, 2000). So typical Red Hill 110 dry sand properties are known as follows; maximum void ratio $e_{\text{max}}=1.035$, minimum void ratio $e_{\text{min}}=0.608$, specific gravity $G_s=2.65$. The six small metal containers were placed in the soil at different locations and depths. The soil was pluviated into the box up to the desired level by using a funnel keeping the same height of fall. The height of fall of the soil was 200 mm for all tests. During each test, the small containers full of the soil were taken and weighted precisely and the natural unit weight of dry soil deposit was calculated.

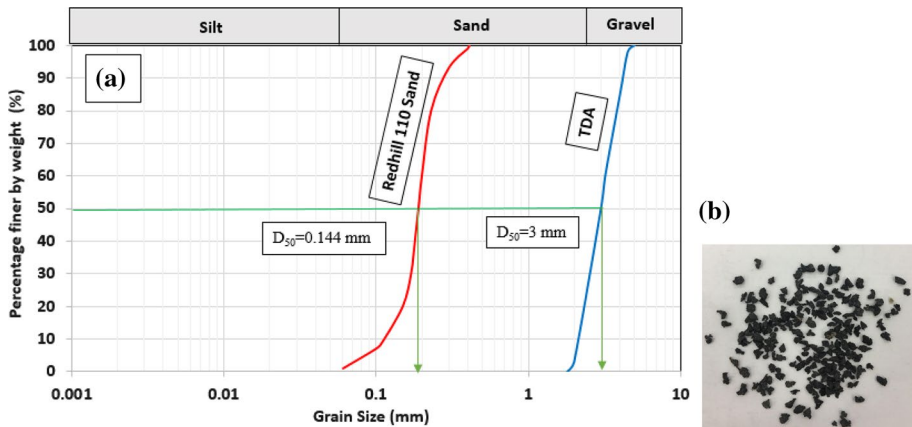


Fig. 2 a Grain size distribution of Red Hill dry sand and TDA, b photos of TDA particles used in the experiments

According to all these parameters obtained from tests mean relative density of Red Hill 110 dry sand was calculated and found as 35%. The physical properties of Red Hill 110 Sand and TDA, also the calculation of relative density in detail can be found at Demirci (2020).

2.2 Physical model setup

Physical modeling is one of the methods to investigate the response of buried pipelines crossing active faults. The various challenges in modeling such problems are well known and the most significant one is the nonlinear behaviour of soils and stress level. The test setup used in the experiments was designed and built by taking the approach which is based on the method suggested in Bhattacharya et al. (2021). In this approach, the governing equation of the problem is written first and then the non-dimensional groups pertaining to the problem are derived from the equation as well as using Buckingham Pi theorem. The physical meaning of non-dimensional groups governing buried continuous pipelines crossing active faults and the values of these dimensionless groups for field and pipelines should be well understood to predict prototype behaviour by using physical model tests. A detailed discussion of non-dimensional groups and scaling laws considered for the design of the test setup can be found in the work of Demirci (2020) and Demirci et al. (2021).

A physical model test setup was developed to simulate buried pipelines crossing strike-slip faults. The side, front, and plan views of the experimental setup are shown in Fig. 3a–c, respectively. The model consisted of two identical boxes such as movable and fixed bases. The total external dimensions of set up are 100 cm width, 200 cm length, and 75 cm depth while the internal dimensions of the model are 95 cm width, 195 cm length, and 70 cm depth. To provide minimum friction and accurate movement, rails, and linear bearings were used to guide and support the movable box. An electrical actuator system was used to laterally displace the box up to a maximum of 30 cm. S-type beam load cell was attached between the tip of the actuator and the movable box to measure the load applied to the box. Wooden plates between the fixed box and movable box were used to prevent the sand from leaking out from the boxes. Pipe insulations foams with 4 cm outer diameter were also placed between the sliding surfaces to prevent the sand from leaking as seen in Fig. 3c. The pipe insulation foams were compressed to provide tightness at the sliding surfaces. As a pipeline model, 170 cm length, 5 cm outer diameter HDPE pipes were used. More details of working principle of the model setup and the specifications of equipment and materials used to construct the setup can be found in Demirci (2020).

The response of model pipelines under strike-slip faulting in terms of longitudinal strains was monitored by using strain gauges along the pipe spring-lines (west and east spring-lines). Figure 4 shows the plan view of the pipeline and the configuration of strain gauges on the pipeline. Analytical method proposed by Sarvanis and Karamanos (2017) predicted the maximum tensile and compressive pipe strains are about 3%. Therefore, the strain gauge range was selected as -3% and $+3\%$ for the experiments. The strain gauges were wired as quarter-bridge. Bending and axial strains are calculated thanks to this configuration. Pipe bending strains (ϵ_b) are calculated as one-half the difference in longitudinal strains between at spring-lines of the pipe, whereas the average of longitudinal strains at spring-lines of the pipe is the axial strain (ϵ_a). A laser displacement sensor was used to measure applied displacements to the movable box throughout the experiments (Fig. 3). A coloured ruler is placed on the upper frame of the movable box, and a marker indicating the 0 value of the ruler is placed on the frame of the fixed box. (see Figs. 5a, 8c 10e). There is also a camera with a bird's eye view of the boxes. The displacement of the movable box

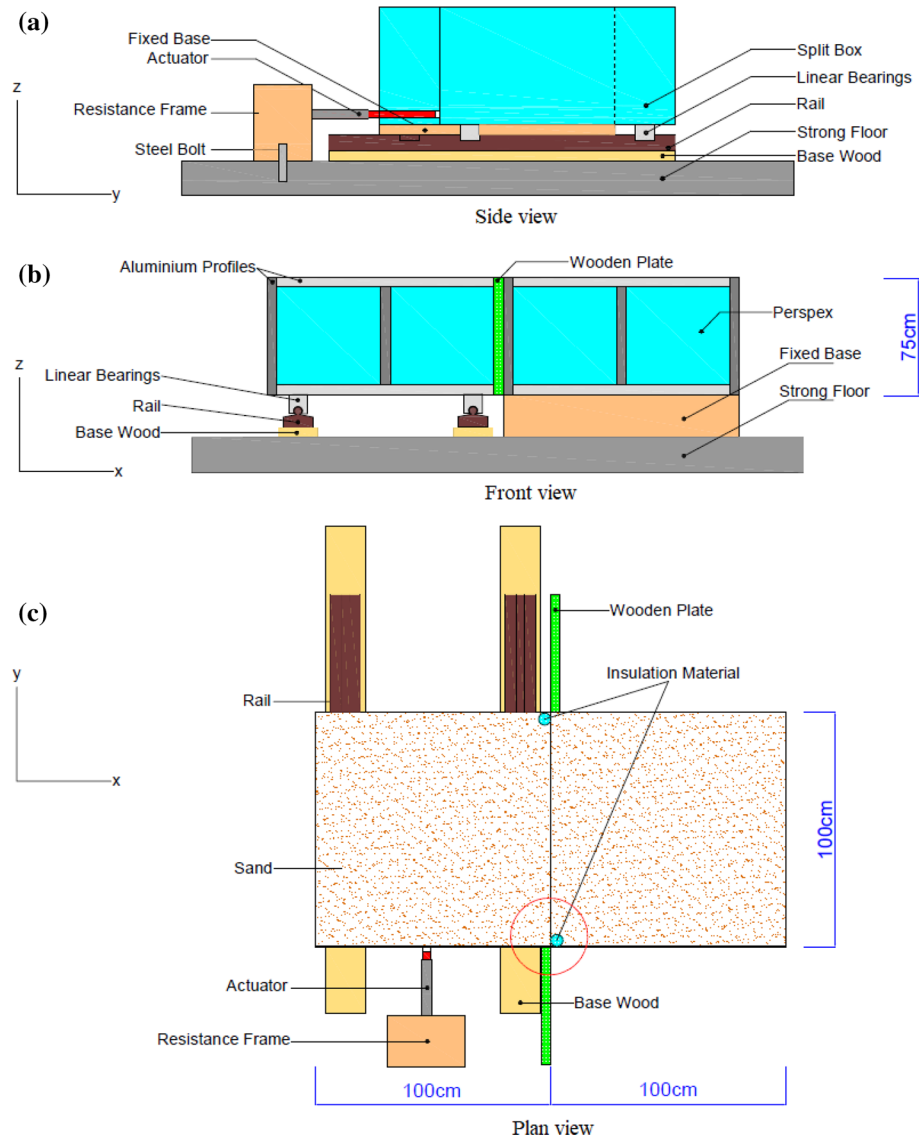


Fig. 3 **a** Side view, **b** front view, and **c** plan view of the experiment setup

by time was recorded by a camera thanks to the moving ruler and fixed marker. The motion is verified by comparison with the laser displacement sensor.

End connectors were used at both ends of the pipe model to represent infinite boundary conditions. End connectors were constructed by using silicon and adhesive mixture. A large number of different adhesive and silicone mixtures were tested (tension and compression tests) to reach the nearly ideal elastic end connector material. Figure 5b shows the force–displacement behaviour of the end connector material used in the experiments. The details of the construction of these end connectors, tension, and compression tests can be

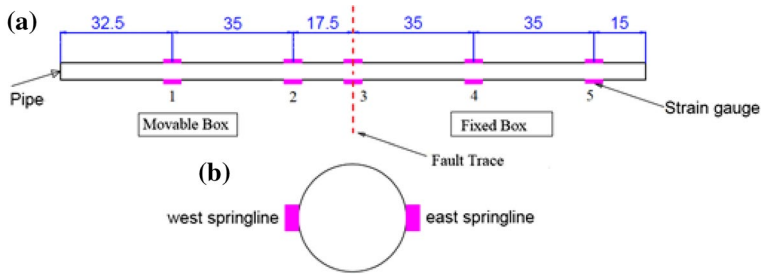


Fig. 4 a Strain gauge layout, and b pipe spring-lines (dimensions in cm)

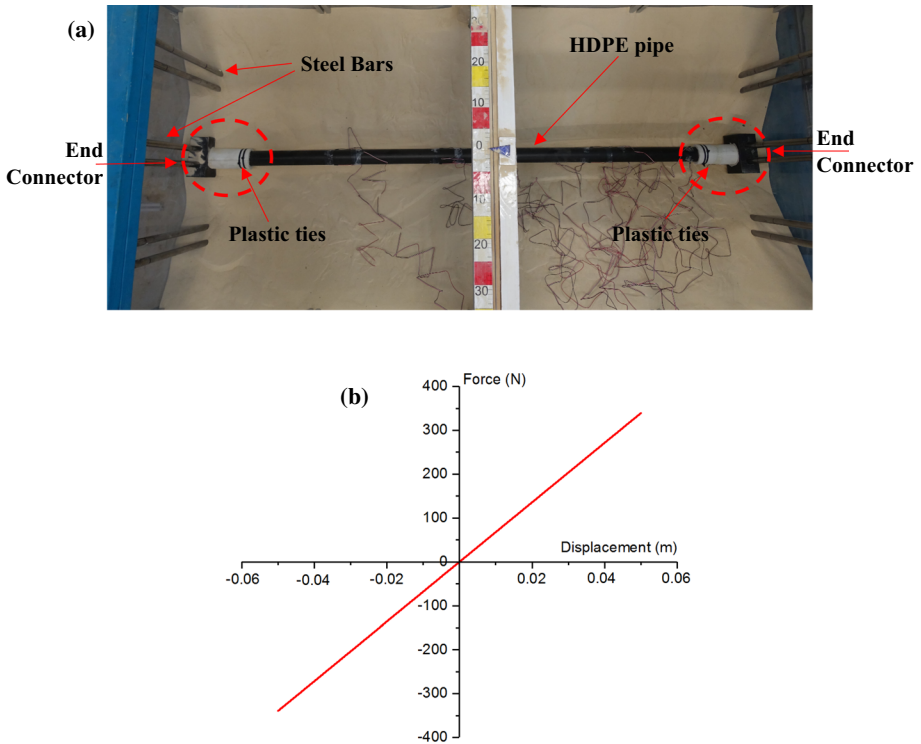


Fig. 5 a The plan view of the experiment setup showing end connectors and plastic ties, b force–displacement behaviour of end connectors

found at Demirci (2020). End connectors are designed to simulate axial soil-pipe interaction along the unanchored length, so they are placed out of the curved zones within the pipeline. The end connector has a negligible rotational stiffness, so it only provides axial continuity at pipe ends.

As shown in the figure, plastic ties were used to attach the pipe to end connectors. Twelve steel bars with a 20 mm diameter were fixed to the base and top of the boxes. The end connectors were placed at both sides of the boxes by using steel bars. It is more efficient to use the steel bars rather than connect the end connectors directly to the box walls

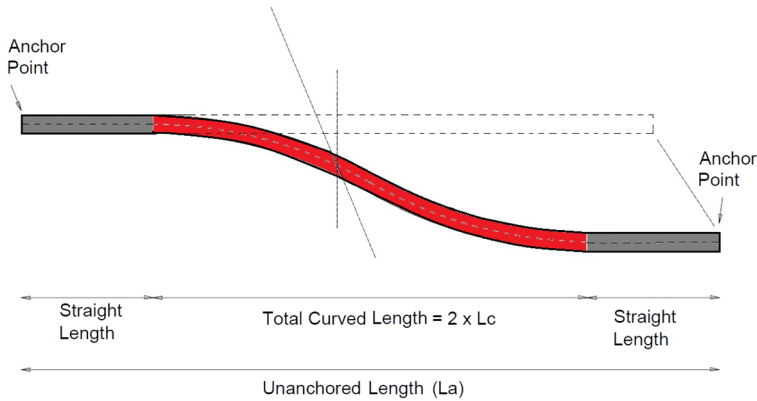


Fig. 6 Schematic sketch of the plan view of a pipeline crossing strike-slip faults

Table 1 Model test plan for seismic mitigation technique—backfilling the pipe with TDA

Test no	Pipe diameter (D), cm	Pipe wall thickness (t), cm	Burial depth (H), cm	Fault crossing angle (β), °	Fault displacement (δ), cm	Percentage of TDA (%)	Trench shape
T-1	5	0.3	35	90	30	0	N/A
T-2	5	0.3	35	90	30	100	Square
T-3	5	0.3	35	90	30	100	Rectangular
T-4	5	0.3	35	90	30	100	Triangular
T-5	5	0.3	35	90	30	50	Triangular

as steel bars allow the pipe to be placed at any desired depth easily and accurately. Also, by using the steel bars, pipeline model can be placed with different angle to fault trace (90° , 60° , 75°). Figure 5a shows the plan view of the experiment setup showing the end connectors, plastic ties, model pipe and steel bars.

Buried pipelines bend at either side of faults as shown in Fig. 6 and curved pipeline sections are therefore developed. The total curved length of the pipeline ($2 \times L_c$) which is also called as high curvature zone should be smaller than the total length of the test setup, which is 2 m, to avoid boundary effects on the global bending behaviour of the pipeline. The curved length over which lateral displacement develops due to curvature (L_c) is a function of fault movement (δ), lateral soil force per unit length (P_u), and pipe bending stiffness (EI) (Sarvanis and Karamanos 2017). The values of $2 \times L_c$ for model tests are calculated by using the analytical methodology proposed by Sarvanis and Karamanos (2017). The calculated values of $2 \times L_c$ are smaller than the total length of the test setup. Readers are referred to the work of Demirci (2020) for details of calculation of the values of $2 \times L_c$ for model tests.

2.3 Model test configurations

Five different physical model tests were performed in this study. As shown in Table 1 the model tests are named as T-1, T-2, T-3, T-4, and T-5. At each of these five tests, the same

size HDPE pipes (5 cm diameter and 0.3 cm wall thickness) were buried at 35 cm depth and the pipes crossed the fault with an angle of 90°. The maximum value of fault displacement used in model tests was 30 cm ($\delta/D=6.0$ where δ is fault displacement and D is pipe diameter). The value of δ/D may reach up to 6 as reviewed case histories in the literature, see the work of Demirçi et al. (2018, 2021). In addition, it was aimed to conduct an experimental campaign to observe the asymptotic response of buried HDPE pipelines so large values of δ/D were considered in the experimental study. In these tests, only the percentage of TDA in the backfill and trench shapes (square, rectangular, triangular) were varied. The pipeline was buried in Red Hill sand in T-1 while model pipelines used in T-2, T-3, and T-4 were placed in a trench that was filled with 100% of TDA. In T-5, the pipeline was buried in a trench with 50% of TDA. The results of T-1 were used as a benchmark to assess the effectiveness of TDA trench applications. Figure 7 shows the schematic view of the trench configuration for each test, along with their dimensions.

At each test, the soil was poured into box by using the funnel, keeping same height of particle fall of about 20 cm. For model tests T-2 and T-3, the steps for the test preparation

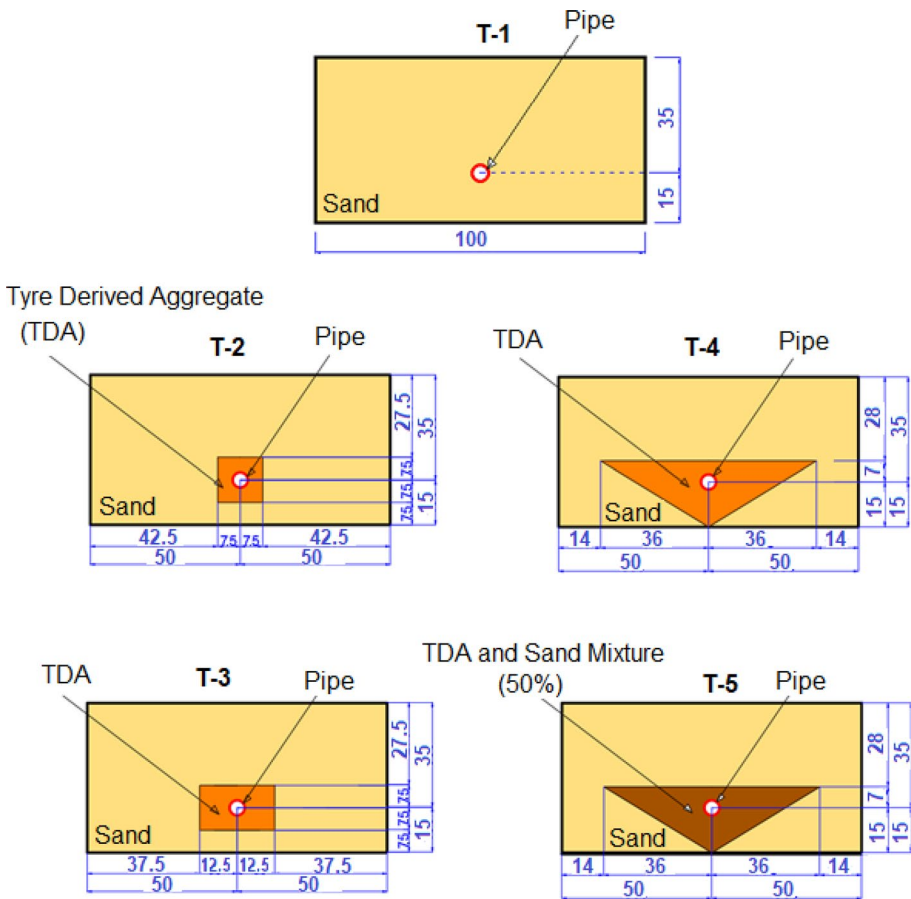


Fig. 7 A schematic view of the trench conditions (TDA content in the trench, trench shape and trench dimensions in cm)

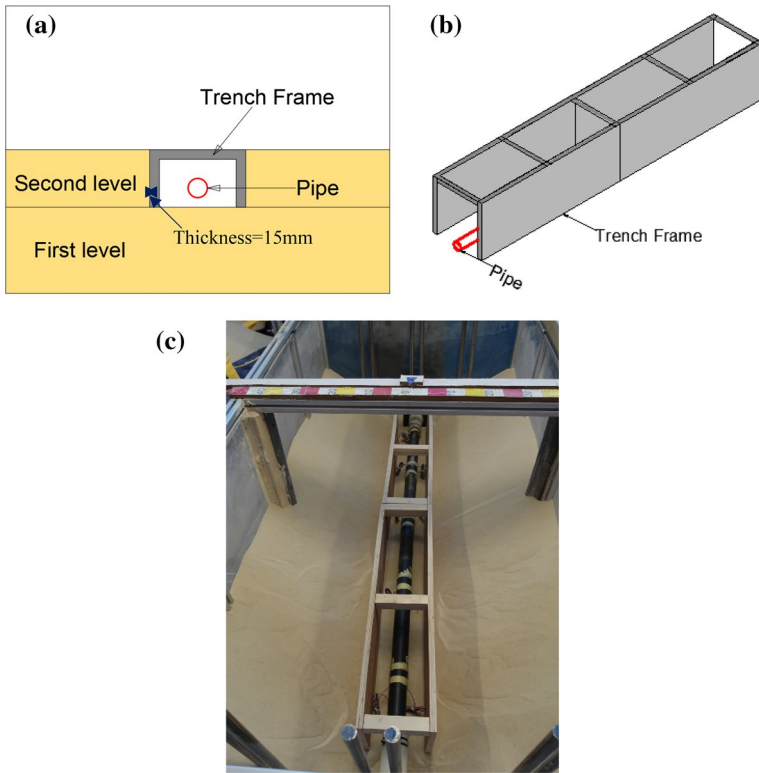


Fig. 8 **a** A schematic illustration showing the placement of trench frame and second-level filling, **b** an isometric sketch of trench frame and **c** a photo of the trench frame and pipeline

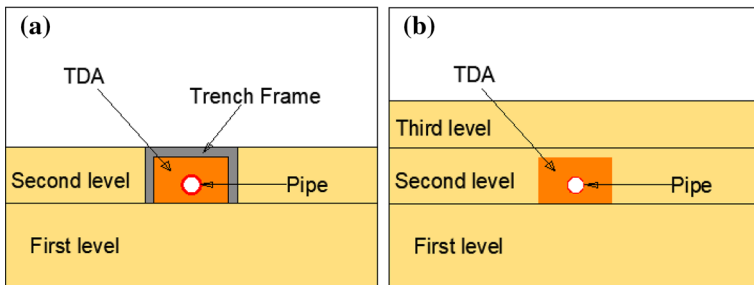


Fig. 9 A schematic illustration showing **a** TDA filling into the trench frame and **b** the removal of the trench and third-level soil filling

are as follows: (1) the Red Hill 110 dry sand was poured into the boxes till 12.5 cm of soil depth was reached. (2) The HDPE pipe was located at 35 cm depth and it was connected to end connectors. (3) The trench frame was placed over the pipeline as shown in Fig. 8a. An isometric sketch of the trench frame is demonstrated as shown in Fig. 8b. Figure 8c shows the photo of the trench frame and placement of pipeline in it. After placing the trench frame, second-level soil filling is performed as shown in Fig. 9a. The trench frame

was constructed from plywood plates which is so light material with a thickness of 15 mm. TDA was poured into the trench frame until the desired level is reached (Fig. 9a). (5) Once TDA filling was completed, the trench frame was removed very slowly. Then, third-level soil filling was performed as shown in Fig. 9b.

For model tests T-4 and T-5, the steps for the test preparation are as follows: (1) A natural trench slope was created as shown in Fig. 10a. The angle of the trench slope was calculated as approximately 31.5° . A trench inclined at a slope (m) of 3:2 was used as proposed by Kouretzis et al. (2013) for sands. Therefore, the trench slope ($m < 3:2$) used in the experiments were considered realistic. (2) Tyre Derived Aggregates (TDA) were poured into trench up to the level of 12.5 cm and then a HDPE pipe was located on the TDA fill as seen in Fig. 10b. Finally, the pipe was linked to end connectors. (3) Second-level of TDA filling was performed as shown in Fig. 10c. The photo of second-level TDA filling is also shown in Fig. 10e) As a last step, final level of soil filling is done as seen in Fig. 10d.

The native ground in the model tests is Red Hill Sand where it could be challenging to excavate an inclined trench wall at a steep angle. A trench inclined at a slope of 3:2 is suggested to be used for sandy native soils in the study of Kouretzis et al. (2013) for simulating

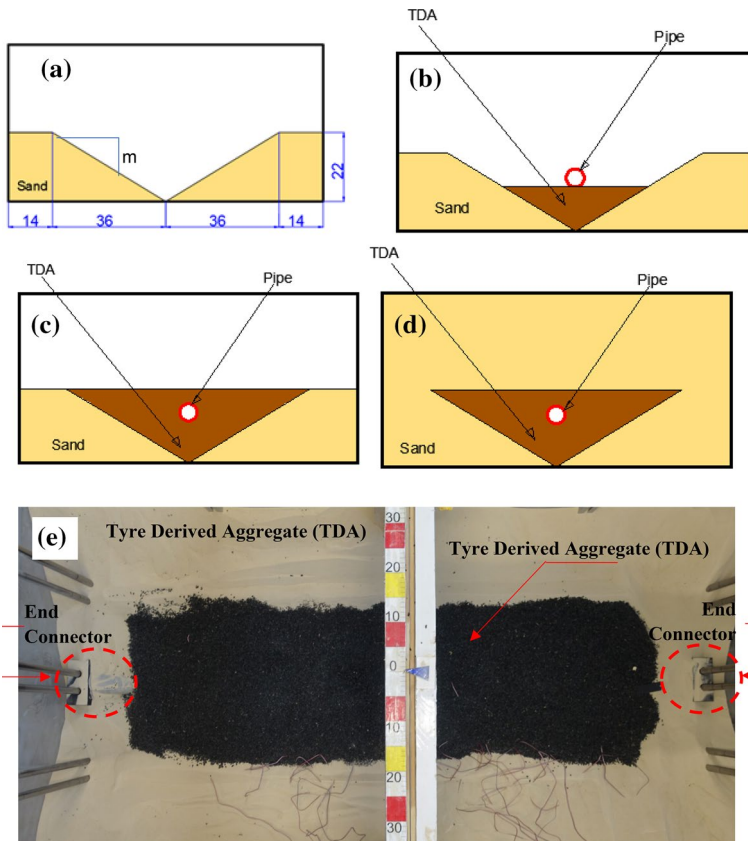


Fig. 10 a A schematic illustration of triangular trench showing its dimensions (all dimensions are in cm), b the first-level TDA filling and placement of HDPE pipe, c the second-level of TDA filling, d the final level of soil filling, and e a photo showing second level TDA filling

more realistic trench conditions. Ni et al. (2018a, b, c) also used a trench inclined at a slope of 3:2 in their numerical study.

3 Model test results

3.1 Axial and bending strain distribution for the model tests

Five pairs of strain gauges were located at spring-lines of the test pipes at different locations. Considering recorded strain data at these locations and displacement profile of the test pipes, it is concluded that test pipes experience double curvature bending under strike-slip faulting. Polynomial trendlines were fitted to data points recorded by strain gauges, and peak bending strains were determined by using these fitted trendlines. Axial strain (ϵ_a) and bending strain (ϵ_b) distributions along the model pipes under various fault displacements ($\delta/D = 1.0\text{--}6.0$) for model tests T-1, T-2, T-3, T-4, and T-5 are plotted in Fig. 11a–e. In Fig. 11a–e at each graph, blue dashed lines show the pipe ends while the red dashed line shows the fault trace. The left-hand side of the fault trace is the movable box and the right-hand side of the fault trace is the fixed box. Figure 11a–e (left-hand column) shows the axial strain distributions along the pipeline for various fault displacements for T-1, T-2, T-3, T-4, and T-5 respectively, while Fig. 11f–j (right-hand column) shows bending strain distributions along the pipeline for various fault displacements for T-1, T-2, T-3, T-4, and T-5, respectively. The curves in each figure represent the trend lines that were fitted to the axial and bending strains measured along the model pipes.

As shown in the figure, for almost all configurations, maximum axial strains develop at the vicinity of the fault trace and it decreases along the pipeline. Peak axial strains developing under 25 cm ($\delta/D = 5.0$) of fault displacement for T-1, T-2, T-3, T-4 and T-5 are 0.26%, 0.18%, 0.16%, 0.097% and 0.23%, respectively. For all model tests, symmetrical double curvature bending, concave on one side of the fault and convex on the other, develops. The bending strains are almost equal to zero at around fault trace. Peak bending strains developing under 25 cm ($\delta/D = 5.0$) of fault displacement for T-1, T-2, T-3, T-4 and T-5 are 1.8%, 1.8%, 1.6%, 1.4% and 2.1%, respectively. It is observed from the axial and bending strain distributions that the percentage of Tyre Derived Aggregate (TDA) in trench backfill, trench shape, and dimensions significantly influence the performance of buried continuous pipelines crossing strike-slip faults.

The axial strains are in the order of 10^{-3} while bending strains are in the order of 10^{-2} as seen in Fig. 11. Considering the magnitudes of axial and bending strains, it is obvious that bending-dominated pipeline response is observed. This behaviour is expected for buried pipelines crossing strike-slip faults with a right angle (see works of Ha et al. 2008; Saiyar et al. 2016; Ni et al. 2018a, b, c).

3.2 Effects of the TDA content and trench shape on the pipeline response to strike-slip faulting

The variation of peak axial strains and peak bending strains for various normalized fault displacements (δ/D) are plotted in Fig. 12. The results of T-1 were used as a benchmark to assess the improvement on the pipe response to strike-slip faulting in terms of axial and bending strains within model pipes.

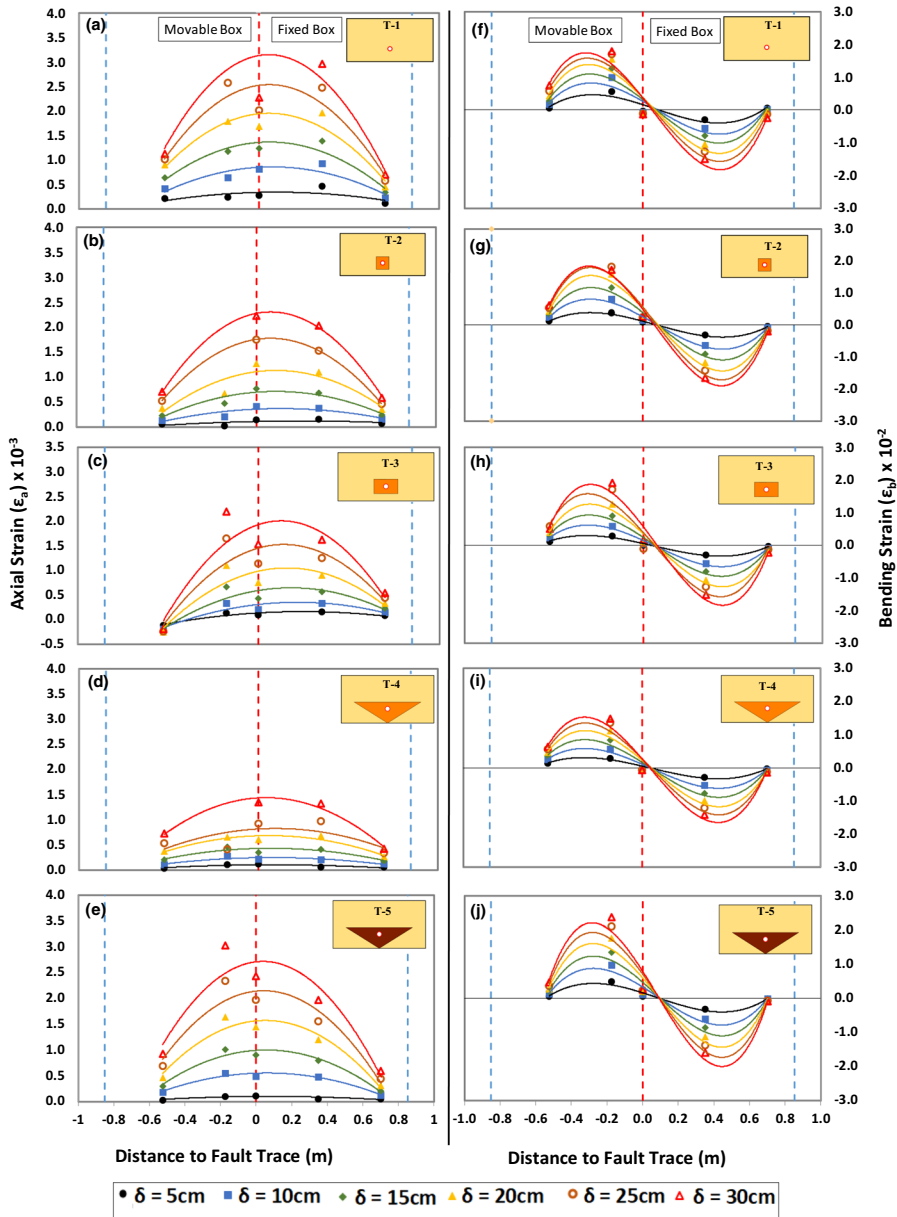


Fig. 11 a-e Axial strain and (f-j) Bending strain distributions along the pipeline for various fault displacements for T-1, T-2, T-3, T-4 and T-5

As observed in Fig. 12a, the smallest axial strains occur under various δ/D for T-4. T-4 is for the model pipeline surrounded by 100% TDA in the triangular trench shape. Peak axial pipe strains decrease with the increase in the content of TDA in the backfill (see T-4 and T-5). Also, trench shape is a significant factor influencing pipe axial strains (see T-4,

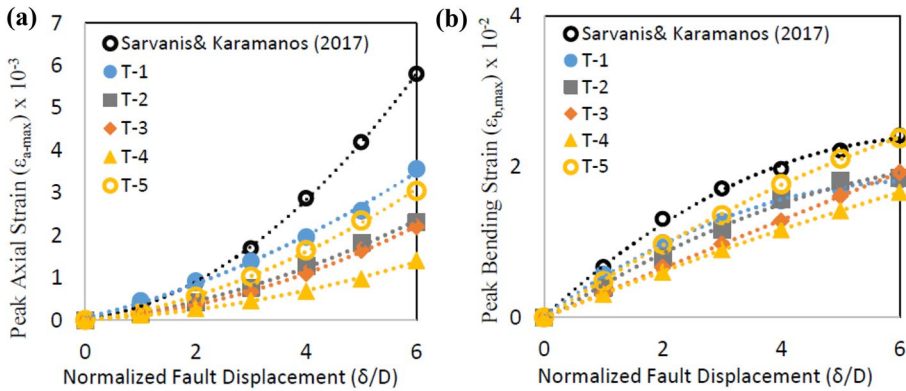


Fig. 12 **a** Peak axial strains vs. normalized fault displacements (δ/D), **b** Peak bending strains vs. normalized fault displacements (δ/D)

T-3, and T-2). Another parameter influencing axial pipe strains is the trench dimensions (see T-2 and T-3).

The variation of peak bending strains for various normalized fault displacements (δ/D) are plotted in Fig. 12b. The minimum peak bending strains develop in T-4 while maximum peak bending strains occur in T-5. The trench shape and percentage of TDA in the backfill influence the pipeline response to faulting in terms of peak bending strains (see T-4 and T-5). Also, trench dimensions are significant parameters affecting the bending response of buried continuous pipelines to faulting. It can be observed by comparing the results of T-3 and T-2 that the increase in the width of the trench decreases pipe peak bending strains in the case of strike-slip faulting.

The peak bending and axial pipe strains obtained by T-1 model test were compared to those values predicted by the analytical method proposed by Sarvanis and Karamanos (2017). Analytical predictions were made for only T-1 model test since strength parameters for TDA such as cohesion and internal friction angle were not studied via laboratory tests in this study. The peak bending and axial strains were calculated for various fault displacements, ranging from 0 to 6 pipe diameter. Lateral soil resistance ($q_{u1} = q_{u2}$) in the analytical method was taken as 2244 N/m for T-1 test and Young's Modulus of the HDPE pipe material was taken as 750 MPa as referenced in the work of Ha et al. (2008). The behavioral trend for peak axial and bending strains recorded in the model tests seems to be consistent with those values predicted by the analytical method. However, the analytical model overpredicts the peak axial and bending strains for T-1 under increasing fault displacements. The measured and predicted peak axial strains are quite close under relatively small fault displacements ($\delta \leq 3D$) while divergence between predicted and measured peak axial strains increases under increasing fault displacements ($3D \leq \delta \leq 6D$). The divergence between the predicted and measured axial strains might occur due to the inadequate stiffness of the pipe end connectors.

Peak axial strains ($\epsilon_{a,max}$) increase exponentially with an increase in normalized fault displacements (δ/D) as observed in Fig. 12a. The increase in fault displacements (δ) increases unanchored length (L_a) of pipelines therefore, peak axial strains increase with an increase in axial forces acting on pipelines. Similar trends for peak axial strains and fault displacements can be observed in the study of Ha et al. (2008). On the other hand, peak bending strains ($\epsilon_{b,max}$) experience a logarithmic increase with an increase in normalized

fault displacements (δ/D) as observed in Fig. 12b. Passive soil failure wedge starts to occur with increasing fault displacements. At a certain fault displacement, the soil in the passive zone fails and the pipe continues to displace through the soil. Since the soil in the passive zone fails, the peak lateral soil-pipe interaction pressure under strike-slip faulting does not increase with increasing fault offset. Therefore, peak bending strains increase very slowly or remain constant with increasing fault displacement. The trends for peak bending strains and fault displacements are similar to those observed in the experimental study of Ha et al. (2008).

Sim et al. (2012) observed that the use of Tyre Derived Aggregate (TDA) trench reduces the pipe bending moments (consequently, pipe bending strains) for relatively small fault displacements ($\delta \leq 1D$). Once the fault displacements exceed one pipe diameter ($\delta > 1D$), the difference between the pipe bending moments in pure sand or in the TDA trench case becomes very small. This is due to that sandy soil comes closer to the pipe after larger fault displacements and mitigation performance of the TDA becomes less significant. In parallel with their study, the mitigation performance of TDA trench in terms of peak bending strains reduced with increasing fault displacement as seen in Fig. 12a. The effect of TDA trench on peak bending strains becomes very small at $\delta = 3D$ for T-2, at $\delta = 5D$ for T-3. The results highlight that the number of sand particles penetrating into TDA increases with increasing fault displacements and this results in a reduction in mitigation performance of TDA trench in terms of peak bending strains.

Ni et al. (2018a, b, c) concluded that enlarging the trench provides a better load reduction for buried pipelines, reducing the risk of pipeline since a wider trench can mitigate the interaction between the stiff native soil outside the trench and buried pipelines. In their study, it is seen that using a trench slope with TDA backfill increases the performance of buried pipelines under strike-slip faulting. This finding is consistent with the experimental results in this study. As seen in Fig. 12, enlarging the trench (comparison between T-2, T-3, and T-4) increases the performance of buried pipelines in terms of both bending and axial strains.

Figure 13a, b shows the variation of peak tensile and compressive strains for various normalized fault displacements. The minimum peak tensile and compressive strains are observed in T-4 while maximum peak tensile and compressive strains develop in T-5. Peak

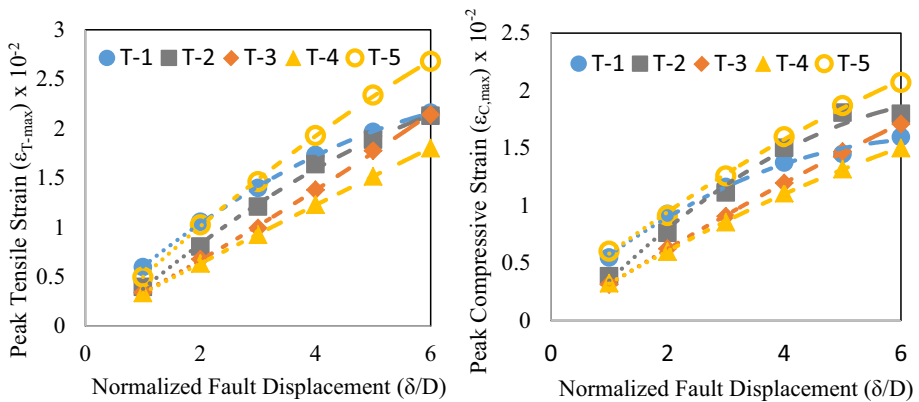


Fig. 13 **a** Peak tensile strains vs. normalized fault displacements (δ/D) and **b** Peak compressive strains vs. normalized fault displacements (δ/D)

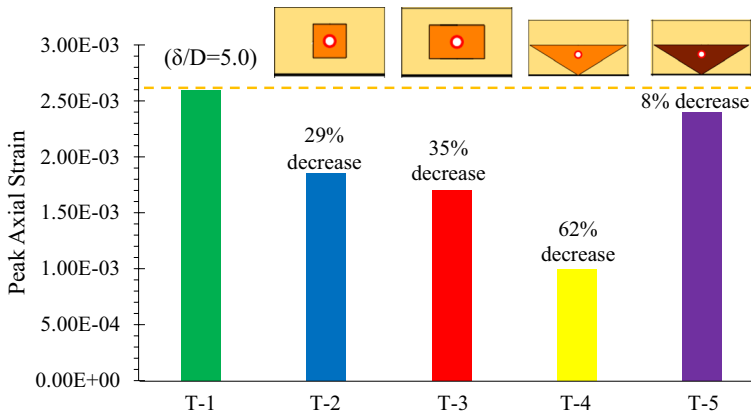


Fig. 14 The variation in peak axial strains for each test with reference to T-1 ($\delta/D=5.0$)

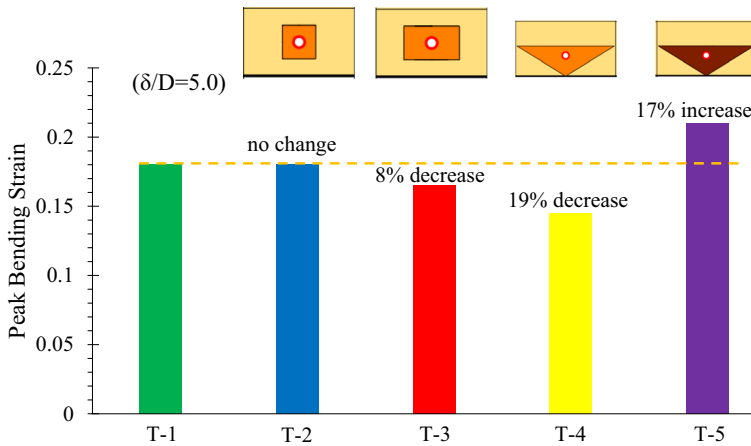


Fig. 15 The variation in peak bending strains for each test with reference to T-1 ($\delta/D=5.0$)

tensile and compressive strains in T-3 and T-4 are very close under relatively small normalized fault displacements ($\delta \leq 3D$) while divergence increases under increasing fault displacements ($3D \leq \delta \leq 6D$). The performance-based design of pipelines is made considering peak tensile and compressive strains developing in pipelines. The potential of local buckling and tensile failure of pipelines buried in a triangular trench backfilled with 100% TDA is reduced since peak tensile and compressive strains are decreased.

Column charts showing the change in peak axial and bending strains for each test with reference to T-1 are plotted in Figs. 14, 15. The peak axial and bending strains in the figures are for $\delta/D=5.0$. As observed in Fig. 14, peak axial strains in each test decrease relative to the results of T-1. The decrease in peak axial strains for T-2, T-3, T-4 and T-5 are 29%, 35%, 62% and 8%, respectively. As seen in Fig. 13, the peak bending strain in T-2 does not change relative to the values in T-1. The decrease in peak axial strains for T-3 and T-4 are 8% and 19%, respectively. In contrast to T-3 and T-4, the peak bending strain in T-5

increases 17% relative to the peak bending strain in T-1. The best performance in terms of reduction in peak axial and bending strains has been observed in T-4.

Overall, the performance of buried pipelines under strike-slip faulting in terms of peak axial strains can be increased up to 62% (see T-4) by using 100% TDA backfill with the sloped trench. The increase in the performance of buried pipelines in terms of peak bending strains is much smaller compared to the performance increase in peak axial strains. Consequently, this mitigation technique is considered as a friction reduction technique and a different technique such as flexible joints method needs to be used to substantially increase pipeline performance in terms of peak bending strains (see Melissianos et al. 2016). The average grain size of the Red Hill dry sand is much smaller than the average grain size of TDA used in the model tests. Consequently, sand particles migrate into the TDA trench during the preparation of the model tests and the application of the fault displacements since sand particles are much finer than TDA particles (see Fig. 2). Soil penetration into the TDA trench reduces pipeline performance under faulting, by increasing both peak axial and bending strains. Wrapping the TDA trench with a cover such as geotextiles may prevent soil particles migrating into the TDA trench and consequently, this measure can increase the performance of buried pipelines compared to that without covering the TDA trench.

Average fault displacement can be around 1–2 m for the majority of the seismotectonic settings depending on seismic moment and fault rupture dimensions. This range of fault displacements means reduced values of the ratio of fault displacement to pipe diameter (δ/D) for pipelines with large diameters. Considering smaller values of δ/D ranging between 0 and 2D can provide a better prediction for large diameter pipelines crossing active faults. At normalized fault displacement of 2D, bending and axial strain values for T-4 and T-3 are quite close. However, Tyre Derived Aggregates with an extended triangular trench appear to be a good solution for real-life applications considering both peak axial and bending strains developing along the pipes.

4 Conclusions

In this study, the efficiency of a seismic mitigation technique by backfilling pipeline trenches with Tyre Derived Aggregates (TDA) was assessed through physical model tests for buried pipelines crossing strike-slip faults. A comparative study was carried out by performing five physical model tests to investigate the effects of various parameters such as TDA content in the backfill, trench shapes, and sizes on the mitigation performance of the proposed technique. Based on the experimental results, the major conclusions are summarized as follows:

1. Peak axial strains can be decreased by a significant amount (62%) by using 100% TDA backfill with the sloped trench. Therefore, the trench backfill with 100% TDA content and a sloped trench are suggested to be used to improve the performance of buried pipelines crossing strike-slip faults.
2. Enlarging the trench is also an effective way to improve the efficiency of the proposed mitigation technique and as a result, it enhances the pipeline performance under strike-slip faulting.
3. The increase in the performance of buried pipelines in terms of peak axial strains is much larger compared to the performance increase in peak bending strains. Therefore, this mitigation technique is considered as a friction reduction technique and a differ-

ent technique such as flexible joints method needs to be used to substantially decrease pipeline peak bending strains developing within pipelines.

4. Soil penetration into the TDA trench leads to a reduction in the pipeline performance under faulting by increasing both peak axial and bending strains in the pipeline. Therefore, it can be suggested that a cover such as geotextiles that prevent the soil from migrating into the TDA trench is used to wrap the trench. This measure may increase the performance of buried pipelines under strike-slip faults compared to that without wrapping the TDA trench with a cover.

Although present study was performed for the pipeline crossing the fault trace with only 90° angle, by using one type of pipe material (HDPE) and one size of (3 mm) TDA; it is believed that the results provide insights into the practical implications of the usage of TDA as a backfill material for buried pipelines.

5 Limitations and suggestions for future studies

5.1 Limitations of the study

Grain size effects on soil-pipe interaction problems can cause a significant issue in physical model tests. The grain size of backfill material should be chosen such that there are no important grain size effects on the response of test pipes crossing strike-slip faults. As seen in the literature, the smallest ratio of the pipe diameter to average soil grain size (D/D_{50}) was chosen considering the criterion of $D/D_{50} \geq 48$ recommended by the International Technical Committee TC2 (2005) based on centrifuge data from Ovesen (1981) and Dickin and Leuoy (1983). In this study, the ratio of the pipe diameter to average TDA grain size ($D_{50, TDA}$) is around 16. Hence, grain size effects on the pipeline response to strike-slip faulting may be significant.

According to design guidelines (ASTM D6270–20, 2020), tire-derived aggregates (TDA) are grouped into two categories based on their particle size: (a) Type A TDA has a particle size of less than 75 mm and (b) Type B TDA has a particle size ranging from 150 to 300 mm. Using Type A TDA as a backfill material will constitute a more uniform contact at the pipe-TDA interface (Ni et al. 2018a, b, c). TDA with large particle size (Type B) tends to compress more under loading with respect to those with TDA having smaller particle size (Type A) (Yi et al., 2015). In addition, TDA with smaller particle size has higher unit weight in consequence of the ease of compaction in the field (Yi et al. 2015). Considering this information, it is anticipated that seismic mitigation performance of backfilling the trench with Type B TDA is higher than backfilling the trench with Type A TDA.

The details of 13 pipeline failure case records were presented in the work of Demirci et al. (2018). As seen in these case records, the diameter of field pipelines ranges from 100 to 2515 mm. Surely, there are pipelines with smaller or larger diameters than these values in the field. The range considered for pipe diameters in the field is considered sufficient to reach a conclusion. The range of values of $\frac{D_{pipe}}{(D_{max})_{TDA}}$ for these pipelines are presented in Table 2, where D_{pipe} is pipe diameter and $(D_{max})_{TDA}$ is the maximum particle size of TDA. As seen in the table, there are four different scenarios shown by roman numbers: (a) Scenario I: small diameter pipes and a trench backfilled with Type A TDA, (b) Scenario II: small diameter pipes and a trench backfilled with Type B TDA, (c) Scenario III: large diameter pipes and a trench backfilled with Type A TDA, and (d)

Table 2 The range of values of $\frac{D_{pipe}}{(D_{max})_{TDA}}$ for field pipelines considering Type A and Type B tire-derived aggregates (TDA)

	Type A TDA	Type B TDA
<div style="display: flex; align-items: center;"> <div style="margin-right: 10px;"> <p style="margin: 0;">Small diameter</p> <p style="margin: 0;">↑</p> </div> <div style="margin-right: 10px;"> <p style="margin: 0;">D=100 mm</p> </div> </div>	$\frac{D_{pipe}}{(D_{max})_{TDA}} > 1.33$ I	$0.33 < \frac{D_{pipe}}{(D_{max})_{TDA}} < 0.67$ II
<div style="display: flex; align-items: center;"> <div style="margin-right: 10px;"> <p style="margin: 0;">Large diameter</p> <p style="margin: 0;">↓</p> </div> <div style="margin-right: 10px;"> <p style="margin: 0;">D=2515 mm</p> </div> </div>	$\frac{D_{pipe}}{(D_{max})_{TDA}} > 33.53$ III	$8.38 < \frac{D_{pipe}}{(D_{max})_{TDA}} < 16.77$ IV
Notes: Type A TDA: $D_{max} < 75 \text{ mm}$ Type B TDA: $150 \text{ mm} < D_{max} < 300 \text{ mm}$ $(D_{max})_{TDA}$: maximum particle size of TDA		

Scenario IV: large diameter pipes and a trench backfilled with Type B TDA. Maximum particle size of TDA used in the experiments, $(D_{max})_{TDA}$, is 5 mm as seen in Fig. 2, corresponding to that the ratio of $\frac{D_{pipe}}{(D_{max})_{TDA}}$ is equal to 10. As seen in Table 2, the ratio considered in the experiments falls within the 1st and 4th scenarios. However, the ratio of the pipe diameter to particle size used in the experiments is not consistent with the real-life applications where large diameter pipes and Type-A TDA are used (scenario 3) and in the real-life applications where small diameter pipes and Type B TDA are used. If the ratio of $\frac{D_{pipe}}{(D_{max})_{TDA}}$ in the field is greater than that considered in the experiments (scenario III for this study), there will be many more interacting TDA particles in the vicinity of the pipeline layout compared to the physical model tests. More interacting TDA materials around the pipeline lead to more uniform contact at the pipe and TDA interface. As reviewed in the literature, small TDA particles have less compressibility and higher unit weight compared to those have large particles. In the light of this information, pipeline strains in the real-life application for scenario III (see Eq. 1) are expected to be larger than the pipeline strains recorded during the model tests. On the other hand, pipeline strains in the real-life applications for scenario II (see Eq. 2) are expected to be lower than the pipeline strains recorded during the model tests.

$$\left(\frac{D_{pipe}}{(D_{max})_{TDA}} \right)_{field} > \left(\frac{D_{pipe}}{(D_{max})_{TDA}} \right)_{model} \tag{1}$$

$$\left(\frac{D_{pipe}}{(D_{max})_{TDA}} \right)_{field} < \left(\frac{D_{pipe}}{(D_{max})_{TDA}} \right)_{model} \tag{2}$$

The peak axial soil force (T_u) acting on the soil-pipe interface is calculated by using Eq. 3, which is proposed in ALA (2001). As seen in the equation, the friction force has two

components: (a) adhesive component (the first part of the equation) and (b) frictional component (the last part of the equation).

$$T_u = \pi D \alpha c + \pi D H \gamma \left(\frac{1 + K_0}{2} \right) \tan f \phi \quad (3)$$

where D is pipe diameter, α is adhesion factor, c is cohesion of the backfill, H is the depth of the soil from the ground surface to the center of the pipe, γ is the effective unit weight of the backfill, K_0 is the coefficient of the lateral pressure, f is a reduction factor depending on the outer surface characteristics of the pipe and ϕ is internal friction angle of the backfill.

Ahn et al. (2015) proposed that an internal friction angle of 22–36° and cohesion of 13–14 kPa for TDA can be used based on the results from direct shear tests (Foose et al. 1996; Moo et al. 2003 and Xiao et al. 2015). El Nagggar et al. (2021) also reported that internal friction angle and cohesion of TDA are in the range of 21–27° and 13–16 kPa, respectively. Therefore, it is obvious that the behaviour of TDA becomes adhesive-frictional under relative soil-pipe movement during faulting. In real-life conditions, the adhesive component of the soil-pipe friction force increases by N (N is the scaling factor, see Eq. 4) since cohesion of TDA and adhesion factor is constant and pipe diameter increases by the value of N . In real-life applications, the frictional part increases by the value of N^2 since pipe diameter (D) and pipe burial depth (H) increase by N . The elongation stiffness of the pipeline increases by the value of N^2 (assuming the same pipe material is used) since it is proportional to the square of the pipe diameter. The total friction force (T_u) acting on the soil-pipe interface will not increase by the value of N^2 since the increase in adhesive component is equal to the value of N . In the lights of these facts, TDA will impose less constraints on the pipeline in the real-life applications with respect to the test setup. Therefore, pipe strains will be lower under faulting in real-life applications compared to the strain values recorded in the experiments.

$$N = \frac{D_{prototype}}{D_{model}} \quad (4)$$

$$N = \frac{H_{prototype}}{H_{model}} \quad (5)$$

Local gauge stiffening (reinforcement) effect is observed when strain gauges are installed on a thin-walled structure or on a structure, even if it is thick-walled, made by a material with a low Young's Modulus (Little et al. 1990; Perry 1985; Ajovalasit et al. 2005). Cholewa et al. (2009) considered an appropriate modification factor (1.3) to scale up the measured strains due to local gauge stiffening/hardening. The local gauge hardening was observed since the stiffness of the strain gauge and adhesive was very close to that of the flexible pipe material used in their study. As seen from the work of Cholewa et al. (2009), it is obvious that local gauge hardening significantly influences the values of strains recorded by strain gauges. However, in the research work of Ajovalasit et al. (2013), the discrepancy between theoretical predictions and experimental results where strain gauges were used to record pipe strains is always less than 2% for pipe materials with Young's modulus greater than 500 MPa. In addition, in the work of Simpson et al. (2015), the measurements from fiber optic sensors were in good agreement with those recorded by conventional strain gauges located on HDPE pipes. These two research studies (Ajovalasit et al. 2013 and Simpson et al. 2015) highlighted that the deviation of strain values (due to local

gauge hardening effect) recorded by strain gauges placed on HDPE pipe remains in a tolerable limit. All in all, the strain values recorded in the model tests are most probably smaller than the strain values that are observed in the field due to the local gauge hardening effect. Therefore, the strain values recorded in the experiments need to be scaled up by using an appropriate modification factor in order to better predict prototype response.

5.2 Suggestions for future studies

Using 50% sand and 50% TDA mixture in the pipeline trench appears not to be efficient since D_{50} of sand is much smaller than the D_{50} value of TDA used in the experiments. Since soil particles migrate into voids between TDA particles under increasing fault displacements as well as even before the fault displacements, the friction reduction effect of TDA becomes negligible. Therefore, it can be suggested to use coarser sand materials ($D_{50, \text{sand}} > D_{50, \text{TDA}}$) to avoid penetration of soil particles into the voids of TDA particles under faulting.

A set of conventional laboratory tests such as pull-out or direct shear tests with different confining pressures can be carried out in future studies to better understand the soil-pipe interface properties. Numerical analyses for risk mitigation purposes can be performed by researchers and engineers by using the interface properties obtained from laboratory tests.

The value of δ/D may reach up to 6 as reviewed case histories in the literature, see the work of Demirci et al. (2018) and Demirci et al. (2021). In addition, it was aimed to conduct an experimental campaign to observe the asymptotic response of buried HDPE pipelines so large values of δ/D were considered in the experimental study. However, the large values of normalized fault displacements may be of little use for design considerations due to extremely high levels of fault average displacement values corresponding to prototype diameter dimension that may become out of the range of seismotectonic context for many countries.

In the scope of this study, there is no investigation carried out in terms of the economy of the seismic mitigation technique. In order to investigate the trade-off between the economy and the benefit of the method in reducing axial and bending pipe strains needs to be studied in future studies.

Acknowledgements The authors wish to thank The Ministry of Education of the Republic of Turkey for their higher education bursary scheme and also The Scientific and Technological Research Council Of Turkey for International Research Fellowship for PhD Students that made it possible to complete this research study at University of Surrey. The authors would like to thank Dr George Nikitas for his help during the experiments.

Funding The 1st author would like to thank to Scientific and Technological Research Council of Turkey (TUBITAK) for the financial support of International Research Fellowship for Ph.D. Students (Grant No: TUBITAK BIDEB 2214-A 2017/2 1059B141700512). The 2nd author is grateful for the higher education bursary scheme provided by The Ministry of Education of the Republic of Turkey.

Declarations

Conflict of interest The authors declare that there is no conflict of interest.

Open Access This article is licensed under a Creative Commons Attribution 4.0 International License, which permits use, sharing, adaptation, distribution and reproduction in any medium or format, as long as you give appropriate credit to the original author(s) and the source, provide a link to the Creative Commons

licence, and indicate if changes were made. The images or other third party material in this article are included in the article's Creative Commons licence, unless indicated otherwise in a credit line to the material. If material is not included in the article's Creative Commons licence and your intended use is not permitted by statutory regulation or exceeds the permitted use, you will need to obtain permission directly from the copyright holder. To view a copy of this licence, visit <http://creativecommons.org/licenses/by/4.0/>.

References

- Ahn S, Cheng L, Fox PJ, Wright J, Patenaude S, Fujii B (2015) Material properties of large-size tire derived aggregate for civil engineering applications. *J Mater Civil Eng* 27(9):04014258. [https://doi.org/10.1061/\(ASCE\)MT.1943-5533.0001225](https://doi.org/10.1061/(ASCE)MT.1943-5533.0001225)
- ASTM D6270–20 (2020) Standard practice for use of scrap tires in civil engineering applications. ASTM International, West Conshohocken, PA. <https://doi.org/10.1520/D6270-20>
- ASTM D4253-00 (2000) Standard test methods for maximum index density and unit weight of soils using a vibratory table. ASTM International, West Conshohocken, PA. <https://doi.org/10.1520/D4253-00>
- ASTM D4254-00 (2000) Standard test methods for minimum index density and unit weight of soils and calculation of relative density. ASTM International, West Conshohocken, PA. <https://doi.org/10.1520/D4254-00>
- Ajovalasit A, Zuccarello B (2005) Local reinforcement effect of a strain gauge installation on low modulus materials. *J Strain Anal* 40:643–653
- Ajovalasit A et al (2013) The reinforcement effect of strain gauges embedded in low modulus materials. *Strain* 49:366–376
- ALA (2001). Guidelines for the design of buried steel pipe, American Lifelines Alliance.
- Bhattacharya, S., Demirci, H.E., Nikitas, G., Prakhya, G.K.V., Lombardi, D., Alexander, N. A., Aleem, M., Amani, S., Mylonakis, G., 2021. Physical modeling of interaction problems in geotechnical engineering. *Modeling in Geotechnical Engineering*. Academic Press, pp. 205–256. <https://doi.org/10.1016/B978-0-12-821205-9.00017-4>. ISBN 9780128212059.
- Cholewa JA, Brachman RWI, Moore ID (2009) Response of a polyvinyl chloride water pipe when transverse to an underlying pipe replaced by pipe bursting. *Can Geotech J* 46(11):1258–1266
- Choo YW, Abdoun TK, O'Rourke MJ, Ha D (2007b) Remediation for buried pipeline systems under permanent ground deformations. *Soil Dyn Earthq Eng* 27(2007):1043–1055
- Demirci HE, Bhattacharya S, Karamitros D, Alexander N (2018) Experimental and numerical modelling of buried pipelines crossing reverse faults. *Soil Dyn Earthq Eng* 114:198–214
- Demirci HE (2020) Experimental and numerical modelling of buried continuous pipelines crossing active faults. PhD Thesis. Department of Civil and Environmental Engineering, University of Surrey, <https://doi.org/10.15126/thesis.00853022>
- Demirci HE, Karaman M, Bhattacharya S (2021) Behaviour of buried continuous pipelines crossing strike-slip faults: Experimental and numerical study. *J Nat Gas Sci Eng* 92:103980
- Dickin EA, Leuo CF (1983) Centrifuge model tests on vertical anchor plates. *ASCE J Geotech Eng* 109(12):1503–1525
- El Naggat H, Zahran K, Moussa A (2021) Effect of the particle size on the TDA shear strength and stiffness parameters in large-scale direct shear tests. *Geotechnics* 2021(1):1–17. <https://doi.org/10.3390/geotechnics1010001>
- ETRMA (2019), The European tyre and rubber manufacturers' association, end of life tyres collected and treated in 2019.
- Foose GJ, Benson CH, Bosscher PJ (1996) Sand reinforced with shredded waste tires. *J Geotech Eng* 122(9):760–767
- Gantes CJ, Bouckovalas GD (2013) Seismic verification of the high pressure natural gas pipeline Komotini–Alexandroupolis–Kipi in areas of active fault crossings. *Struct Eng Int* 23:204–208
- Gantes CJ, Melissianos VE (2016) Evaluation of seismic protection methods for buried fuel pipelines subjected to fault rupture. *Front Built Environ* 2:34
- Hasegawa N, Nagamine H, Imai T (2014) Development of steel pipe for crossing fault (SPF) using buckling pattern for water pipelines. *JFE GIHO* 31:61–65
- Honegger DG, Nyman DJ, Johnson ER, Cluff LS, Sorensen SP (2004) Trans-Alaska pipeline system performance in the 2002 denali fault, Alaska. *Earthq Earth Spectra* 20:707–738
- International Technical Committee TC2 (2005). Catalogue of scaling laws and similitude questions in centrifuge modelling.

- Karamanos SA, Keil B, and Card RJ (2014) Seismic design of buried steel water pipelines. In: Proceedings of the pipelines 2014: from underground to the forefront of innovation and sustainability. ASCE, Portland, OR, USA, pp 1005–1019. <https://doi.org/10.1061/9780784413692.091>
- Kouretzis GP, Sheng D, Sloan SW (2013) Sand–pipeline–trench lateral interaction effects for shallow buried pipelines. *Comput Geotech* 54:53–59
- Ha et al. (2008): Buried high-density polyethylene pipelines subjected to normal and strike-slip faulting—a centrifuge investigation
- Little EG, Tocher D, O'Donnell P (1990) Strain gauge reinforcement of plastics. *Strain* 26:91–98
- Melissianos VE, Korakitis GP, Gantes CJ, Bouckovalas GD (2016) Numerical evaluation of the effectiveness of flexible joints in buried pipelines subjected to strike slip fault rupture. *Soil Dyn Earthq Eng* 90:395–410
- Melissianos VE, Lignos XA, Bachas KK, Gantes CJ (2017) Experimental investigation of pipes with flexible joints under fault rupture. *J Constr Steel Res* 128:633–648
- Mokhtari M, Alavi Nia A (2015) The influence of using CFRP wraps on performance of buried steel pipelines under permanent ground deformations. *Soil Dyn Earthq Eng* 73:29–41
- Moo-Young H, Sellasie K, Zeroka D, Sabnis G (2003) Physical and chemical properties of recycled tire shreds for use in construction. *J Environ Eng* 129(10):921–929
- Ni P, Moore ID, Take WA (2018a) Distributed fibre optic sensing of strains on buried full-scale PVC pipelines crossing a normal fault. *Geotechnique* 68(1):1–17
- Ni P, Qin X, Yi Y (2018b) Use of tire-derived aggregate for seismic mitigation of buried pipelines under strike-slip faults. *Soil Dyn Earthq Eng* 15:495–506
- Ni P, Qin X and Yi Y (2018c) Numerical study of earth pressures on rigid pipes with tire-derived aggregate inclusions. *Geosynthetics Int* 25 (5).
- Ovesen NK (1981). Centrifuge Tests of the Uplift Capacity of Anchor. *Proceeding of the tenth international conference on soil mechanics and foundation engineering, Stockholm, pp.712–722.*
- Perry CC (1985) Strain gage reinforcement effects on lowmodulus materials. *Exp Tech* 9:25–27
- Saiyar M, Ni P, Take WA, Moore ID (2016) Response of pipelines of differing flexural stiffness to normal faulting. *Geotechnique* 66(4):275–286
- Sarvanis GC, Karamanos AS (2017) Analytical model for the strain analysis of continuous buried pipelines in geohazard areas. *Eng Struct* 152:57–69
- Sim WW, Towhata I, Yamada S (2012) One-g shaking-table experiments on buried pipelines crossing a strike-slip fault. *Geotechnique* 62:1067–1079
- Simpson B, Hoult NA, Moore ID (2015) Distributed sensing of circumferential strain using fiber optics during full-scale buried pipe experiments. *J Pipeline Sys Eng Pract*. [https://doi.org/10.1061/\(ASCE\)PS.1949-1204.0000197](https://doi.org/10.1061/(ASCE)PS.1949-1204.0000197)
- Trifonov OV, Cherniy VP (2016) Application of composite wraps for strengthening of buried steel pipelines crossing active faults. *ASME J Press Vessel Technol* 138:060902
- Vazouras P, Karamanos SA, Dakoulas P (2010) Finite element analysis of buried steel pipelines under strike-slip fault displacements. *Soil Dyn Earthqu Eng* 30(11):1361–1376
- Xiao M, Ledezma M, Hartman C (2015) Shear resistance of tire-derived aggregate using large-scale direct shear tests. *J Mater Civ Eng* 27(1):04014110
- Yi Y, Meles D, Nassiri S, Bayat A (2015) On the compressibility of tire-derived aggregate: comparison of results from laboratory and field tests. *Can Geotechnic J* 52(4):442–458. <https://doi.org/10.1139/cgj-2014-0110>
- Zhang J, Liang Z, Zhang H, Feng D, Xia C (2016) Failure analysis of directional crossing pipeline and design of a protective device. *Eng Fail Anal* 66:187–201